Onset of the Mid-Miocene Climatic Optimum: inferences from stable isotopes on benthic foraminifera at ODP Site 1264 in the southern Atlantic

April, 2013

Master thesis project

Mischa Saes

Supervisors

Lucas Lourens

Helen Beddow

Universiteit Utrecht

“The most exciting phrase to hear in science, the one that heralds the most discoveries, is not "Eureka!", but "That's funny..."”

Isaac Asimov

Content

Abstract

In 2011, stable isotope records of benthic foraminifera from Ocean Drilling Program Site 1264 have been presented. To gain more knowledge about high resolution early to middle Miocene climate changes, these Oligocene-Miocene records have been extended in this paper. The extended records span the interval from ~18.91 to 16.97 Ma. The $\delta^{18}O$ record exhibits a sharp decrease around 17 Ma, identified as the onset of the Mid Miocene Climatic Optimum (MMCO). The cause of the MMCO is not fully understood, but recent research indicates that it is related to a sharp increase in the atmospheric CO_2 level. The carbon isotope record shows a significant increase from ~17.8 to 16.97 Ma, which is the result of the Monterey event, a period of global CO_2 drawdown. By applying spectral- and wavelet analysis to stable oxygen and carbon isotope records, a very strong, continual imprint of the long term (~400 kyr) eccentricity cycle on the amplitudes of the oxygen and carbon isotope records has been identified. Besides the long term eccentricity cycle imprint, a much weaker imprint of short term (~100 kyr) eccentricity cycle on the amplitudes of the carbon and oxygen isotopes record has been recorded. This data is compared to the stable oxygen and carbon isotope records from the Site 926 and Site 1090. As a result, the Miller events Mi-1ab and Mi-1b have been identified within this interval. The changes in the eccentricity cycle, the oxygen and carbon isotope records of Site 1264 match well, although a phase lag ~43 kyr is identified for the long term eccentricity amplitudes variations of the carbon isotope record compared to the oxygen isotope record. This suggests a coupling between climatic changes and changes in the carbon and oxygen isotope records.

1 Introduction

The earth's climate is an ever changing system. There is a delicate balance between different variables, e.g. solar input, continent configuration, atmospheric CO_2 level and weathering rates, which govern the heating or cooling of Earth's climate. During the Cenozoic, Earth's climate has experienced a significant amount of cooling, including many periods of glaciation, alternated with periods experiencing a considerable amount of heating (Zachos et al., 2001b). During the late Oligocene and early Miocene, there were brief periods when major ice sheets were present on Antarctica (e.g. the Miller events, Miller et al., 1991), although the earth experienced a less cold period compared to the early Oligocene. The mid-Miocene is characterized by two major events, the Mid-Miocene Climatic Optimum (MMC) and the Monterey event (positive carbon isotope excursion). The MMCO is one of the most recent episodes (~17 – 15 Ma) of global warming without human influence (Flower and Kennett, 1994; Zachos et al., 2001b), which makes it an important analogy for the current situation. Currently, the atmospheric CO_2 level is rising with a high rate, which will cause a significant amount heating of Earth's (local) climate. As a result, the earth's current "ice house climate" will turn into a "greenhouse climate" (IPCC 2007).

1.1 Aim of this study

By generating high resolution $\delta^{18}O$ records, the influence of Milankovitch cycles on the formation of large scale Antarctic ice sheets has been proved (Zachos et al., 2001b). This paper will discuss OPD Site 1264. Site 1264 was been drilled in 2003 as part of Leg 208, and is located on the Walvis Ridge (29° S), in the south eastern Atlantic ocean. Site 1264, 2505 m depth, has been drilled as a shallow water depth end-member of the Walvis Ridge (Zachos et al., 2004) (figure 1). In 2011, the benthic foraminifer species *Cibicidoides mundulus* has been used to generate continuous high resolution (<3 kyr) stable carbon and oxygen isotope records (~24 to 18.91 Ma) (Liebrand et al., 2011). In this paper, the records will be extended from ~18.91 to 16.97 Ma, where the onset of the MMCO and the Monterey event might be captured. Since the role of the global carbon cycle during the MMCO is still unclear, the relation between the changes in the global carbon cycle and the oxygen isotope record (represents both ice volume and temperature) of Site 1264 during

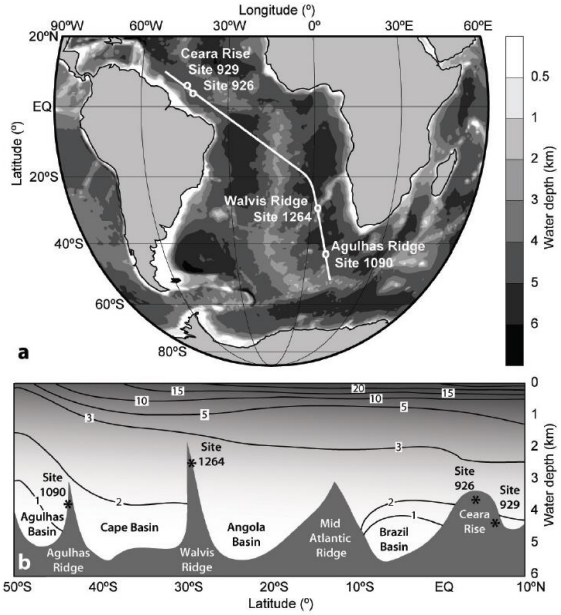

Figure 1. A. Location of the different well sites. The white line represents the transect through the different well sites, shown in figure b. B. Transect through the different well sites, latitude and depth are of the different sites are shown. Black lines represent the current day water depth.

the onset of the MMCO will be studied. The Mi-1ab and Mi-1b events, which have occurred during the extended interval, will be linked to the oxygen isotope record. The previous study of Site 1264 pointed out the dominance of both the eccentricity cycles during the Oligocene and early Miocene (Liebrand et al., 2011). For the extended part of both records, the influence of the different Milankovitch cycles, especially long term (~400 kyr) and short term (~100 kyr) eccentricity cycles, on the amplitudes of these extended isotope records will be studied. The records will be compared to the composite record of ODP Site 1090 (hole D and E), from the Agulhas ridge (43° S), 3699 m water depth (Billups et al., 2004) and to the record of ODP site 926 (Hole B) from the Ceara Rise, Equatorial Western Atlantic, 3598 m water depth (Pälike et al., 2006) (figure 1).

2 Background

2.1 Ocean water reorganisation and ice sheet formation

The $\delta^{18}O$ records from different sites indicate a long-term (from the Eocene to the present) ocean interior cooling trend. The total global ice volume shows a continued increase in ice volume from the Eocene to present, with major expansions and contractions of the Arctic and Antarctic ice sheets (Zachos et al., 2001b and Cramer et al., 2009). The $\delta^{18}O$ record reveals three major stages in polar ice sheet formation. First stage: glaciation of Antarctica during the earliest Oligocene (33-34 Ma), Oi-1 event of Miller (1991). Second stage: permanent East Antarctic ice sheet development during the Middle Miocene, (12 - 14 Ma), (Wright et al., 1992; Flower and Kennett, 1994). Third stage: increase of large scale Northern Hemisphere ice sheets during the late Pliocene (2.6 – 2.7 Ma), (Shackleton et al., 1984; Cramer et al., 2009). Miller et al. (1991), distinguished seven Miocene oxygen isotope events in the $\delta^{18}O$ record, called Mi-1 to Mi-7 (and a few "sub events"), the Mi-1 event occurred during the relatively warm late Oligocene en early Miocene period. These events are characterized by increased oxygen isotope values of ~2.0 ‰. Substantial Antarctic ice volume increases are predicted for the bases of Mi-2, Mi-3 and possibly Mi-5 events, resp. 16.1, 13.6 and 11.3 Ma. Zachos et al. (2001b), also report a glaciation during Mi-1, ~23.9 Ma. Liebrand et al. (2011) used a 1D model to show that, on long term and short term eccentricity time scales, polar cooling and ice-sheet growth during the modelled period occurred almost simultaneously. This model predicts an Antarctic ice sheet configuration change from the half to the full present day situation during the Mi-1 event at ~23 Ma. A global sea level of about 2.5 m above the present day situation was the result of the west and east Antarctic ice-sheets reaching their maximum size, which shows that the ice-sheets had almost the same size as the present day ice sheets (Pekar and DeConto 2006; Liebrand et al., 2011). Ice volumes of 50 to 125 % of the present day East Antarctic Ice Sheet have been predicted for the early Miocene (23 – 17 Ma) (Pekar and DeConto, 2006).

The continued cooling of the ocean interiors and the increase in ice volume since the Eocene resulted in the reorganisation of the ocean interior. A switch from a homogeneous to a heterogeneous ocean state is revealed from interbasinal comparisons (Cramer et al.,

Table 1. Calculated atmospheric CO_2 levels by different methods and different studies.

Author	Method	CO_2 level (ppm)
Sheldon (1997)	Paleosol model	2 – 3 times current level
Kürschner et al. (2008)	Stomatal frequency	~ 500
Pearson and Palmer (2000)	$\delta^{11}B$	~ 250
Foster et al. (2012)	$\delta^{11}B$	350 – 400
Pagani et al. (1999)	$\delta^{13}C$ and $\delta^{18}O$	190 – 260
Royer et al. (2001)	Leaf stomatal index / partial CO_2 pressure	300 – 450
You et al. (2009)	Model	460 - 580

2009). This could be the result of decreased sensitivity of ocean water density to ocean temperature differences due to a low temperature of oceans (below 4.5 °C) (De Boer et al., 2007). During the Oligocene/Miocene, the oceans became more homogeneous while the ocean temperatures remained above 4.5 °C (6 -7 °C) (Lear et al., 2000), which indicates it is not the result of a decreased sensitivity of the ocean water. During the Miocene, the distribution of bottom water masses was probably significantly different from today (Pekar and DeConto, 2006). $\delta^{18}O$ data suggests that, in the interval ~22 – 17 Ma, the warmest waters were present in the tropical Indian Ocean. Site to site benthic foraminifer $\delta^{18}O$ comparison shows that during the latest Oligocene and the early Miocene, $\delta^{18}O$ gradients were present between the North and South Atlantic, which provides evidence for the formation of relatively warm, deep waters in the North Atlantic. This water reached the deep tropical Atlantic, but it did not reach the Southern Atlantic (Billups et al., 2002). Cramer et al., (2009) suggest that the geographic pattern of the δ18O differentiation during the Oligocene/Miocene is the result of the development of the Antarctic Circumpolar Current (ACC). In an ocean without the ACC, thermally driven currents would only be confined to the upper few hundred meters in most parts of the ocean (Toggweiler and Samuels, 1998). A significant amount of early-Miocene variability in the production of proto-AABW (Antarctic Bottom Water) is suggested by the δ18O record of Site 1090. It is suggested that during the Mi-events (glacial maxima), the production of proto-AABW from the cooling of surface waters and the formation of sea-ice was enhanced because of the close proximity of ice-sheets to the coastline, this influenced the d18O record of Site 1090 (Pekar and DeConto, 2006).

2.2 The Mid-Miocene Climatic Optimum and the Monterey Event

The Mid-Miocene is a period (~17.0 – 15.0 Ma) characterized by low Antarctic ice volume (25 – 70 % of present day east Antarctic ice-sheet) increased temperatures, the Mid-Miocene Climatic Optimum (MMCO) (Wright et al., 1992; Flower and Kennett 1994; Pekar and DeConto, 2006). It is estimated that temperatures were about 6 °C higher, relative to the present, during the maximum intensity of the MMCO (Flower and Kennett, 1994). A recent study shows that the earth's surface reached a global mean temperature as high as 18.4 °C during the MMCO, which is about 3 °C higher than the current mean surface temperature (You et al., 2009). The cause of the MMCO is still under discussion (Pagani et al., 1999; Mosbrugger et al., 2005; Kürschner et al., 2008).

The atmospheric CO_2 level has been related to MMCO, although its role is still unclear. Low atmospheric carbon dioxide levels during the MMCO have been derived from carbon isotope/boron isotope studies from deep ocean cores (pCO_2 of 190 – 260 ppm), (Pagani et al., 1999; Pearson and Palmer, 2000). This is in contradiction to the findings of Kürschner and Kvaček (2009), who related Central European floral assemblages to the a relatively high atmospheric CO_2 level. Cowling (1999) suggested high CO_2 levels too as a cause of the MMCO, based on the prediction of photosynthetic models. This is in agreement with the earlier findings of Kürschner et al. (2008). Kürschner et al. (2008) used stomatal frequencies to reconstruct a relatively high middle Miocene atmospheric CO_2 level.

Higher than current atmospheric carbon dioxide levels have also been suggested by Sheldon (2006), who modelled carbon dioxide variations to simulate the formation of a specific type of paleosols, which suggests that 2 to 3 times current CO_2 level was necessary. Royer et al. (2001) suggested, based on the inverse relation between the leaf stomatal index en the partial CO_2 pressure, a carbon dioxide level comparable to the current carbon dioxide level. A recent study based on a planktonic foraminiferal $\delta^{11}B$ record (Foster et al., 2012) indicated a much higher MMCO CO2 level than Pearson and Palmer (2005).

To test the sensitivity of the climate system to changes in the atmospheric carbon dioxide level and other variables, different computer models have been evaluated (table 1). These models show that an increase in CO_2 level results in warming of the climate, and high latitudes will warm more than low latitudes (Tong et al., 2009; Henrot et al., 2010 and You, 2010). Tong et al. (2006) simulated that other driving mechanisms but a CO_2 increase, cannot simulate a reduced temperature gradient between the tropics and the poles. Henrot et al. (2010), show that a warmer climate at all latitudes during the mid-Miocene can only be simulated with an atmospheric carbon dioxide level higher than the current level. Local warming is produced with changes in sea surface conditions and lowering of the topography. Warm and humid conditions might have been maintained and intensified by changes in vegetation cover (Henrot et al., 2010). You (2010), modelled the MMCO and discovered that northern and southern polar temperatures are driven by different mechanisms. The model does support the idea that higher than modern carbon dioxide levels were necessary to cause the global temperature rise during the MMCO.

The middle Miocene stable en carbon isotope record is characterized by a significant increase around 16 Ma (Cramer et al., 2009), termed the Monterey event (Flower and Kennett, 1993b). The Monterey event (17 - 12 Ma) consists of 5 or 6 individual carbon isotope peaks. The Monterey event is thought to be related to global cooling through drawdown of atmospheric CO_2 during the middle Miocene, the "Monterey hypothesis" (Flower and Kennett, 1993; Vincent and Berger, 1985), this might however in be in contradiction with the MMCO.

3 Material and methods

3.1 Measurements

Every 2 cm, samples of approximately 10 g of sediment were taken from ODP site 1264. These samples from were freeze dried and washed in tap water and sieved at 38, 63 and 150 µm fractions. The samples were dried in evaporation basins. Before picking, the 150 µm fraction was dry-sieved to obtain the fraction larger than 250 µm. From this fraction, one to twenty specimen of the foraminifer species *Cibicidoides mundulus* were picked. In the case no specimen could be found, the >150 µm or a dry sieved >212 µm fraction of the sample was analysed for forams of the same species *(Cibicidoides mundulus)*. The chosen fraction for picking, depended on the amount of forams in the >150 µm fraction.

For every sample, about one to five of the most undamaged specimen were chosen for analysis. These samples were ultrasonically cleaned in ethanol, for the samples with sufficient specimens (two or more), the sample was crushed before ultrasonically cleaning in ethanol.

At the Faculty of Geosciences of Utrecht University, stable oxygen isotopes ($\delta^{18}O$) and stable carbon isotopes ($\delta^{13}C$) were measured for every sample. Foraminiferal tests with a mass between 20 – 60 µm were dissolved in a Finnigan MAT Kiel III automated preparation system. Isotopic ratios of purified CO_2 gas were measured on-line with a Finnigan MAT 253 mass spectrometer and compared to an internal standard. The Utrecht University in-house standard "Naxos" and the standard NBS-19 were used to calibrate the results to the Vienna Pee Dee Belemnite (VPDB). The $\delta^{18}O$ values were corrected for the disequilibrium of the sea water by adding 0.64 ‰ to the $\delta^{18}O$ values (Shackleton, 1974). For 19 samples, a duplicate was measured. By calculating the standard deviation, a reproducibility (95% confidence interval) of 0.28 ‰ for $\delta^{18}O$ and 0.35 ‰ for $\delta^{13}C$ was calculated (attachment 1). The high numbers

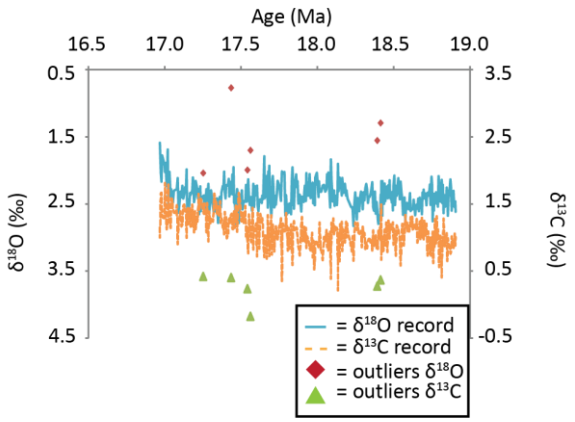

Figure 2. Carbon and oxygen isotope records and the removed outliers. Outliers have been removed by eye.

for reproducibility are probably because of the small amount of duplicates. Outliers were removed by eye. Six outliers were identified (figure 2). Because the analysis of stable oxygen and carbon isotopes is paired, outliers were removed from both records. After the removal of outliers, the carbon and oxygen isotope records of Site 1264 consist of 397 data points. Of these data points, 282 data points correspond to Hole A, the remaining 115 data-points correspond to Hole B (attachment 2).

3.2 Age Model

The age model of site ODP 1264 is based on magnetostratigraphic data. Since the magnetostratigraphy of site 1264 is incomplete, the magnetostratigraphy of the nearby ODP 1265 site is used. The patterns of the magnetic susceptibility (MS) and colour reflectance (CR, 600 / 450 nm) of the ODP site 1264 records are matched to records of ODP site 1265 (Liebrand et al. 2011). The Astronomical Tuned Neogene Time Scale 2004 (ATNTS2004) ages (Lourens et al. 2004) are assigned to the magnetic reversals and a third order polynomial function is used to inter- and extrapolate this age model (Liebrand et al. 2011). To test the validity of the age model the $\delta^{18}O$ and $\delta^{13}C$ records have been compared to the lascar (2011) curve (Laskar et al., 2011).

3.3 Analytical methods

To calculate difference between different records for the period ~17 – 19 Ma, the records are resampled, with a step of 2 kyr, and the three point averages of these resampled records are calculated. The equally spaced, smoothened records, are subtracted from each other, which results in a graph showing the difference between to records. Next, spectral analysis is applied and the data has been filtered, both by using the software package AnalySeries (Paillard et al., 1996).
In order to be able to apply wavelet analyses, both records have been de-trended by using a notch filter (frequency: 0.0 kyr^{-1} and a bandwidth of 0.02). After re-sampling of the data (2.0 kyr time step), matlab has been used to create a wavelet plot. By using the software package AnalySeries (Paillard et al., 1996), the phase relation for the different components (identified by spectral analysis) has been determined.

4 Results

4.1 Overall trends

4.1.1 MMCO and Monterey event

The extended carbon and oxygen isotope records (~18.91 – 16.97 Ma) connect well to the records by Liebrand et al. (2011) (figure 3). $\delta^{18}O$ amplitudes vary between ~1.8 and 2.8 ‰. The oxygen isotope record exhibits a clear negative trend from ~17.3 to 16.97 Ma (figure 4c). During this time, $\delta^{18}O$ values decrease from 2.4 ‰ to about 1.75 ‰. Both Zachos et al. (2001b) and Cramer et al. (2009) report a negative shift of oxygen isotopes ~18 - 17 Ma. Between ~16 and 14 Ma, a ~2 Myr minimum with values between ~1.5 – 1.85 ‰ is reported (Zachos et al., 2001b and Cramer et al., 2009). This minimum is the Mid Miocene Climatic Optimum (MMCO) (Zachos et al., 2001b). Since the onset of the negative shift of the Site 1264 oxygen isotope record occurs at ~17.34 Ma, combined with comparable minimum values, it is very likely that the negative shift for the Site 1264 $\delta^{18}O$ record is the onset of the MMCO. By means of lithostratigraphic analysis of ANDRILL core AND-2A, the onset of the MMCO is identified by Fielding et al. (2011) which shows a close match to the onset

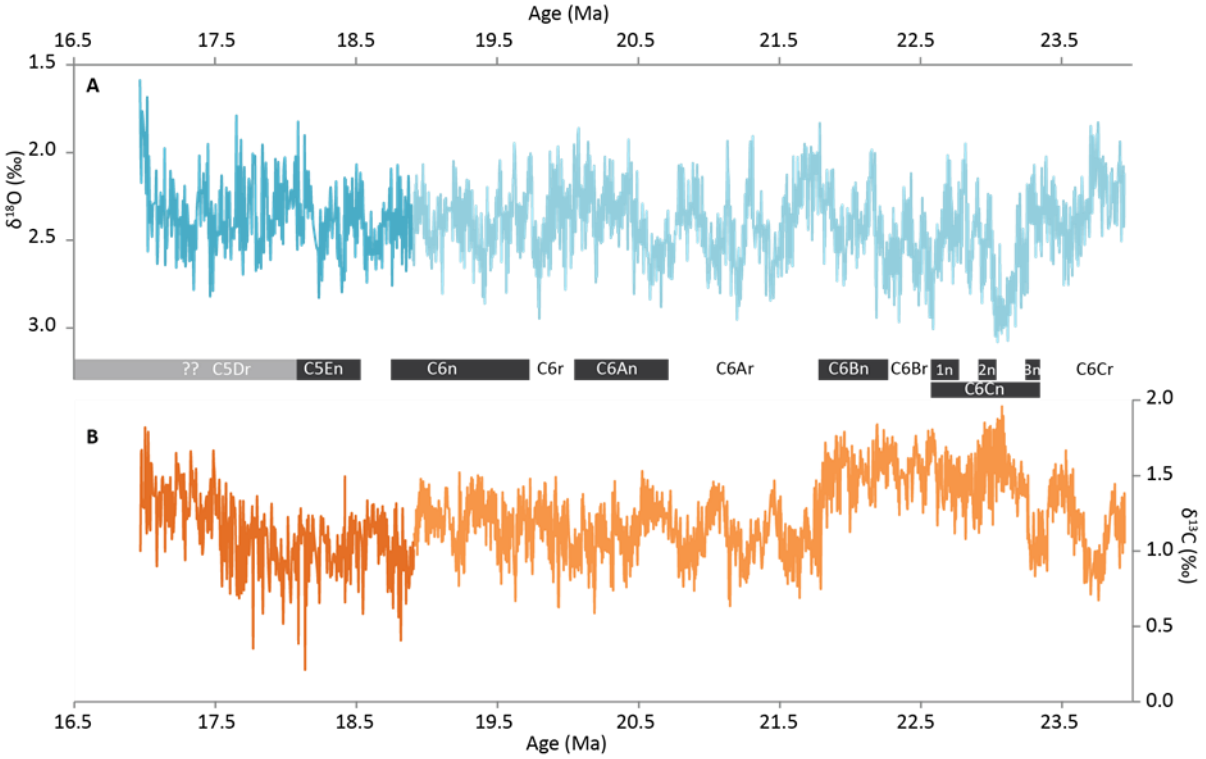

Figure 3. The extended records of Site 1264. A. Complete oxygen isotope record. Light blue; δ18O record from ~24 – 19 Ma (Liebrand et al., 2011). Dark blue; $\delta^{18}O$ record from ~19 – 17 Ma. B. Same as A., only $\delta^{13}C$ instead of $\delta^{18}O$. Between A. and B., magnetostratigraphy from Site 1265 (Bowles, 2006).

record by this study (~17.35 Ma compared to 17.34 Ma).

From ~18.9 to 17.8 Ma, the carbon isotope record exhibits a trend similar to the oxygen isotope record, with minima and maxima occurring in conjunction. From ~17.8 Ma to ~17 Ma, there is a gradual increase in carbon isotope values from 1.0 ‰ to about 1.7 ‰ (figure 4d). A significant increase in carbon isotope values during the mid-Miocene is also reported by (Zachos et al., 2001b and Cramer et al., 2009). They both present a shift from ~ 0.75 ‰ to ~ 1.6 ‰ between ~18 to 16 Ma, which leads to a ~3 Myr carbon isotope maximum between ~16 and 13 Ma, the "Monterey event" (Cramer et al., 2009). The onset of the deposition of the Monterey Formation is identified at 17.8 Ma (Flower and Kennett, 1993). The comparable timing of the onset of the event, combined with a similar magnitude is a very strong indication that the onset of Monterey excursion is present in the Site 1264 carbon isotope record. Consequently both the oxygen and carbon isotope records exhibited a distinct shift in isotope values towards ~17 Ma. There are two differences; first, $\delta^{18}O$ record exhibits a positive trend while the $\delta^{18}O$ record exhibit a negative trend, while the $\delta^{13}C$ record exhibits a positive trend; second, the shift in $\delta^{13}C$ values initiates ~17.8 Ma, while the shift in $\delta^{18}O$ values initiates ~17.3 Ma. This implies that the carbon isotope shift leads the oxygen isotope shift.

4.1.2 Comparison to other Atlantic sites

The $\delta^{13}C$ records of Site 1264 and Agulhas Ridge Site 1090 (Billups at al., 2004) match well, with a similar overall trend and coinciding maxima and minima (figure 5b). The "positive" shift in the $\delta^{13}C$ record of Site 1264, initiating at ~17.8 Ma, is also exhibited by the $\delta^{13}C$ record of Site 1090. This shift begins at ~17.6 Ma, ~200 kyr earlier. The δ18O records of the sites 1090 and 1264 show a similar trend with decreasing δ18O values from ~17.3 to 16.97 Ma (figure 5a). Although both records show a negative trend, the $\delta^{18}O$ record of the Site 1264 record exhibits the onset of the MMCO at ~17.34 Ma, while a comparable negative trend initiates at ~17.26 Ma at Site 1090 . The $\delta^{18}O$ records of the sites 926 and 1264 match well, although the $\delta^{18}O$ record Site 926 is generally lower than those of the sites 1090 and 1264.

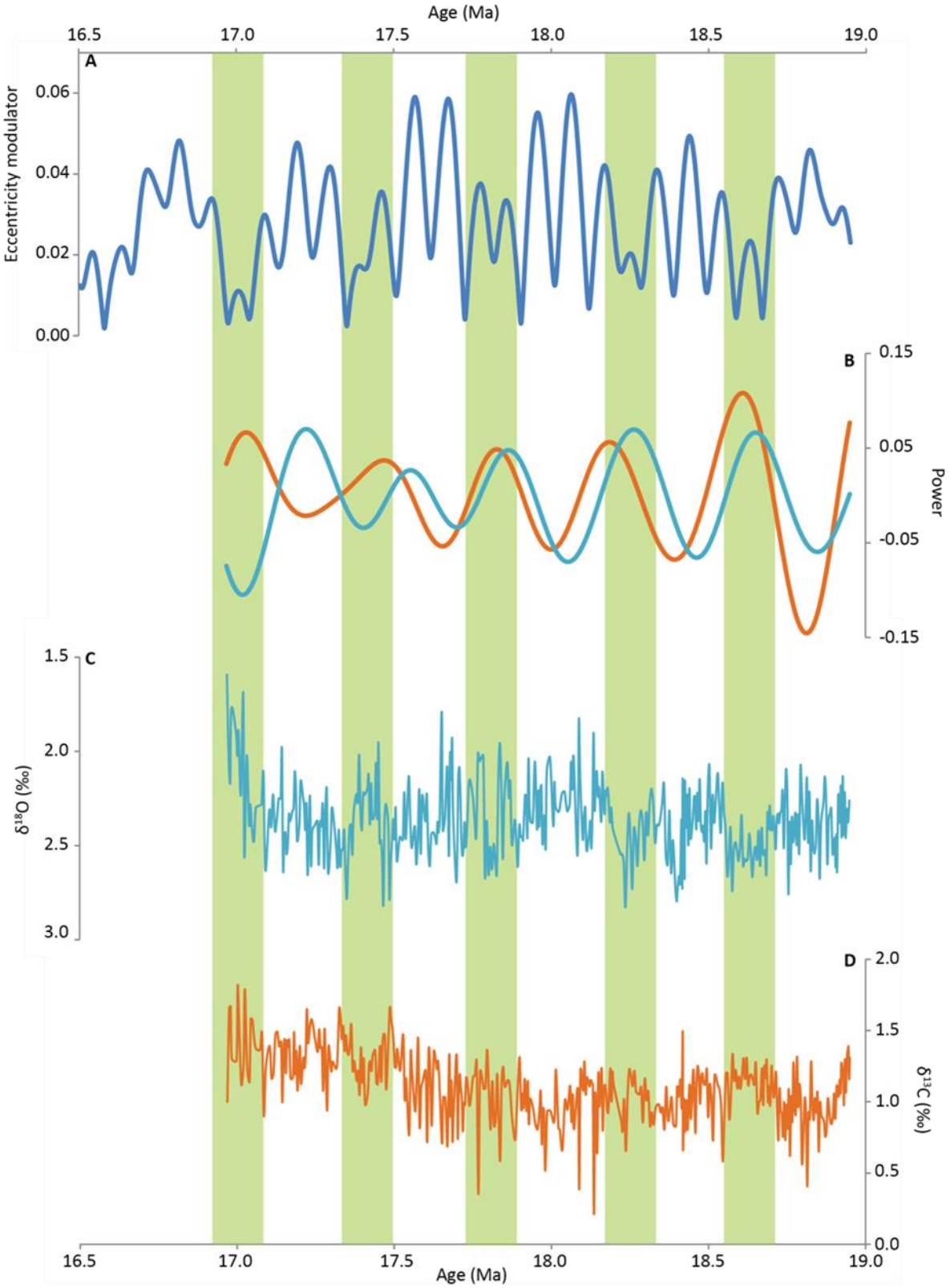

Figure 4: Comparison of: A. Eccentricity modulation (Laskar et al., 2011). B. Gaussian filters (Paillard et al., 1996) (400 kyr, *f*: 2.5, bw: 1.0) of the $\delta^{18}O$ (blue) and $\delta^{13}C$ (orange) records. C. Oxygen isotope ($\delta^{18}O$) record from Site 1264. D. Carbon isotope ($\delta^{13}C$) record from Site 1264.

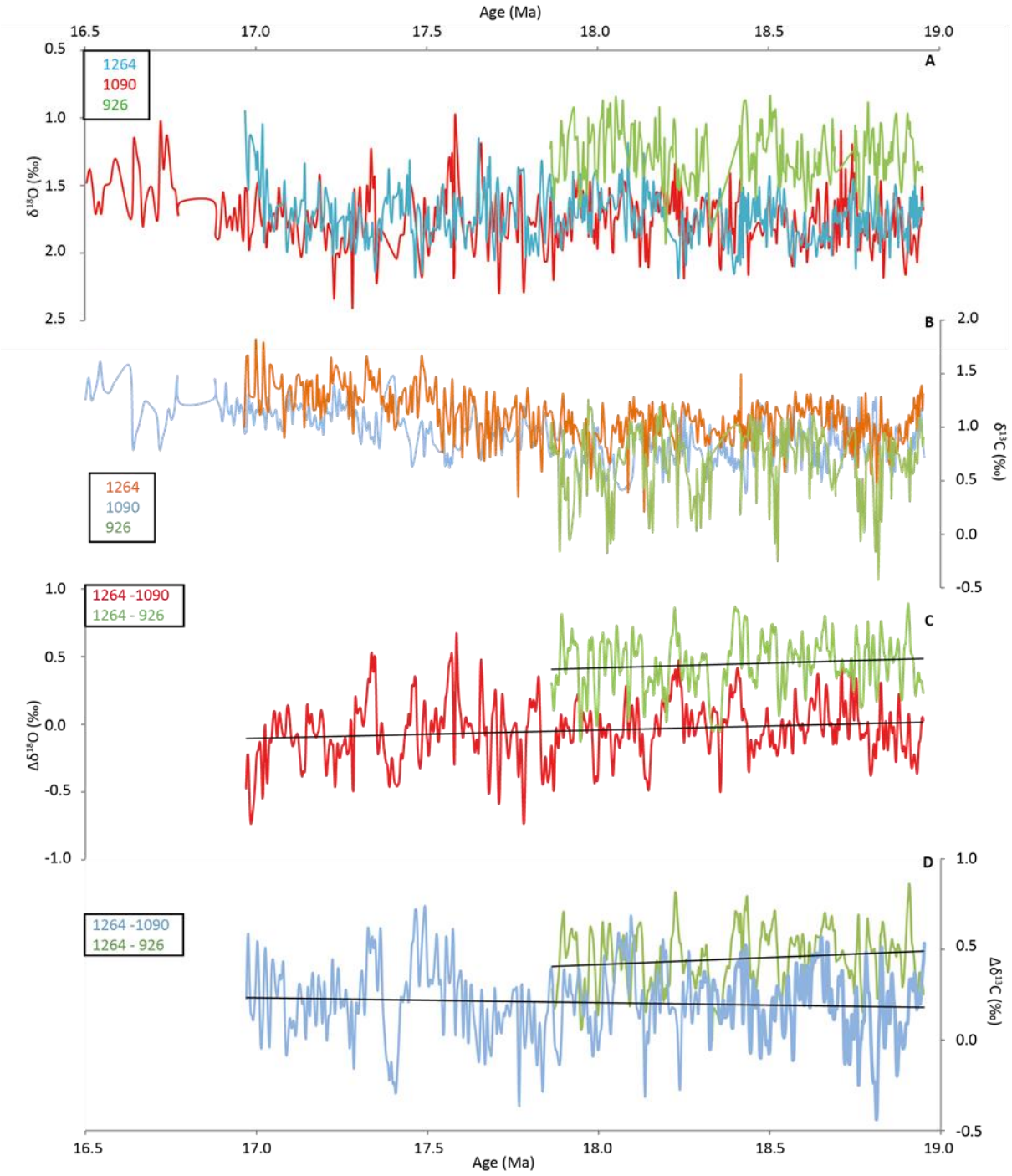

Figure 5. Comparison of early to mid-Miocene stable isotope records from different sites. This includes stable isotope records of Site 1264, Site 1090 and Site 926. A. The $\delta^{18}O$ (+0.64‰) records of the different sites. B. $\delta^{13}C$ records of different sites. C. $\Delta\delta^{18}O$ of different sites (1264 – 1090 (red) and 1264-926 (green)), which indicates the differences between the different records. D. As in (C), but with $\Delta\delta^{13}C$.

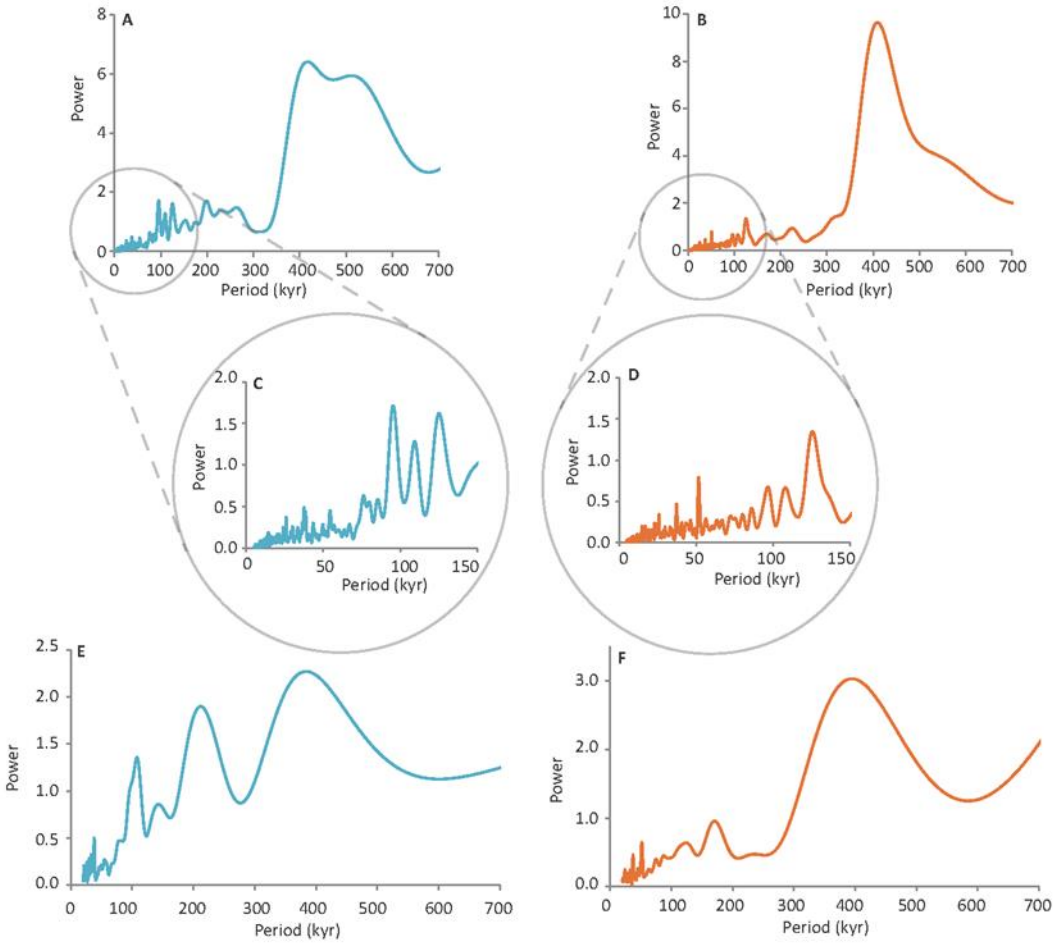

Figure 6. Power spectral analysis. A-D: interval ~24 – 17 Ma. E and F: interval ~20 – 17 Ma. (Paillard et al. (1996). A,C,E: power spectra for the oxygen isotope $\delta^{18}O$ record, B, D, F: power spectra for the carbon isotope $\delta^{13}C$ record.

By subtracting records from different sites, Liebrand et al. (2011) notes a difference of about ~0.5 ‰ between the oxygen isotope record of Site 1264 and of Site 926. By calculating the difference between the different sites for the period ~19 – 17 Ma, a difference of ~0.5 ‰ between the $\delta^{18}O$ records of sites 1264 and 926 has been identified too (figure 5c). The $\delta^{18}O$ record of Site 1264 is generally higher than the record of Site 926. Towards ~17 Ma, this difference decreases gradually to a value of about 0.4 ‰ (figure 5d). The δ13C records of both the Sites 926 and 1090 records are generally lower than the $\delta^{13}C$ record of Site 1264 (figure 5d).

4.2 Spectral analysis and filtering

4.2.1 Spectral analysis

Because the length of the record might influence the result of the outcome of the mass spectral analysis, I chose to present two different time-periods on which power spectral analysis is applied (figure 6). Power spectra the stable isotope data for the time-period 24.0 – 16.97 Ma, focussing on the entire record of Site 1264, and power spectra for the time-period 20.0 – 16.97 Ma, focussing on the extended part of the record, are calculated.

4.2.2 Power spectral results (~24 – 17 Ma)

For both the carbon isotope record as well as the oxygen isotope record, the dominance of the long-term (~400 kyr) cycle is indicated by the power spectral analysis (figure 6a-d). For both the $\delta^{18}O$ record and the $\delta^{13}C$ record,

additional peaks are also found at the short-term (~95 and ~125 kyr) eccentricity cycles. For shorter periods, the peaks are less clear. For both the carbon and oxygen isotope records, power spectral analyses indicates possible obliquity related influence on both records (peaks at respectively ~56 and ~39 kyr). The obliquity influence is to a lesser degree than the eccentricity related influence (figure 6).

4.2.3 Power spectral results (~20 – 17 Ma)

Similar to the long period spectral results, a dominance of the long term eccentricity cycle in both records is detected. The power spectral analysis has also revealed a peak for the oxygen record at ~ 111 kyr and much smaller peaks around 40 kyr, which are the consequence of short-term eccentricity and obliquity modulation respectively. A peak at 200 kyr is also identified. For the carbon isotope record, a peak is found at ~ 125 kyr, which results from short term eccentricity modulation, and another peak is detected at ~ 38 kyr, very close to the obliquity period. For both periods on which power spectral analysis is applied, the long-term eccentricity cycle appears to be much more dominant than the short-term eccentricity and obliquity cycles. This is in agreement with the findings of Liebrand et al. (2011). Although the sampling resolution is well above the nyquist frequency, there are no signs of influence of the precession cycle. Spectral analysis is also applied for Site 926, which revealed a stronger imprint of the obliquity signal, although the long and short term eccentricity cycles are present too (Pälike et al., 2006).

4.2.4 Filtering

The δ13C and $\delta^{18}O$ records have filtered for different periods. They are filtered for periods of 400, 100 and 40 kyr. The non-filtered records are compared to the filtered records.

4.2.5 Long-term eccentricity cycle

Although the applied filter has a broad bandwidth, both filtered records exhibit the long-term (~400 kyr) eccentricity cycle, with ~7.5 cycles in ~2.5 Myr. The filtered and the unfiltered records match well, which emphasizes the importance of the long-term eccentricity cycle for the mid-Miocene (figure 4b). A slight mismatch between the filtered records and the original records is observed after the initiation of the MMCO en Monterey event. The modulated eccentricity, the filtered (long-term eccentricity) $\delta^{18}O$ and $\delta^{13}C$ records are compared, the green bands show the minima in eccentricity modulation (figure 4a – 4b). Six of these minima occur in a period of 2 million years, which means they occur every 400 kyr. When comparing the orange ($\delta^{13}C$ record) and blue ($\delta^{18}O$) lines, it becomes clear the two records are almost in phase, although the maxima in the carbon isotope record lag the maxima in the oxygen isotope record. This was also noted by Liebrand et al. (2011). Overall, the maxima in the filtered $\delta^{18}O$ and $\delta^{13}C$ records seem to occur during minima in the eccentricity modulation, especially between 19.0 Ma and 17.8 Ma. At some moments, the maxima in $\delta^{18}O$ seem to slightly precede the minima in the 400 kyr modulated eccentricity. This is a consequence of the Antarctic ice sheets expanding predominantly during the declining phase of the long term eccentricity, which leads to increase of the oxygen isotope values (Liebrand et al., 2011). Between ~17.3 to 17.0 Ma, the two records behave in a opposite way, possibly due to the onset of the Monterey event and the MMCO. Another possibility is that the age model is wrong in this part of the record

4.2.6 Short-eccentricity and obliquity cycles

Both the d13C record and d18O record match well to the records filtered for the 100 kyr eccentricity related variability. For both original records, the match with the records filtered for the 40 kyr related eccentricity cycle is less profound, although certain individual peaks seem to match. The analysis of these different records indicates a connection between the different astronomical cycles and the oxygen and carbon isotope records, the long-term and short-term eccentricity cycles in particular. For the $\delta^{13}C$ record, the interval ~19.0 to 17.8 Ma is dominated by the long-term eccentricity related variability. During the interval ~17.8 to 17.0 Ma, and the interval ~17.5 and 17.0 Ma in particular, the dominance of the long-term eccentricity related variability is less profound. This interval is much more dominated by the short-term eccentricity cycle.

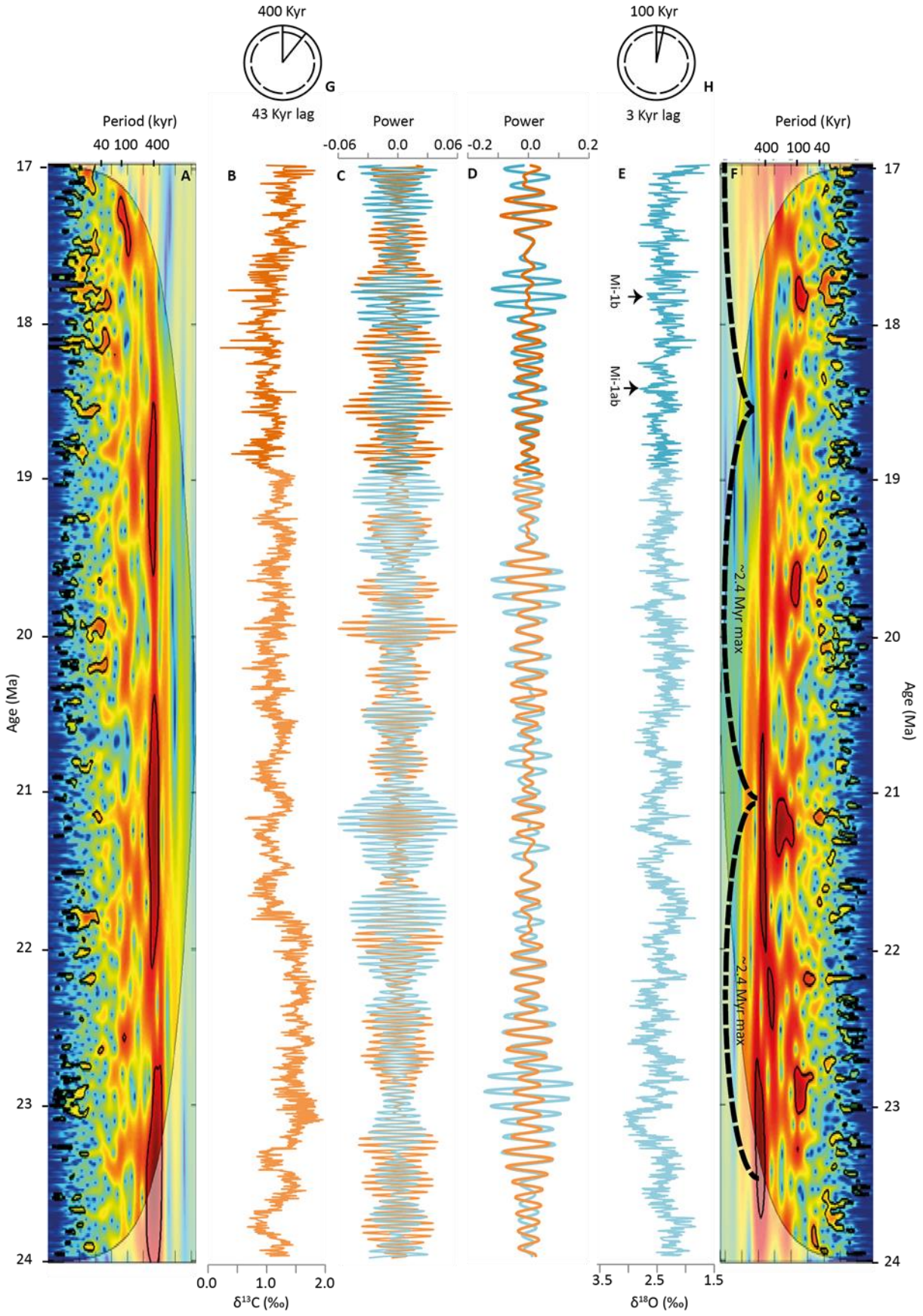
400 Kyr
G
43 Kyr lag
100 Kyr
H
3 Kyr lag
Period (kyr)
40 100 400
Power
-0.06 0.0 0.06
Power
-0.2 0.0 0.2
Period (Kyr)
400 100 40
A
B
C
D
E
F
Mi-1b
Mi-1ab
~2.4 Myr max
~2.4 Myr max
Age (Ma)
17
18
19
20
21
22
23
24
0.0 1.0 2.0
δ13C (‰)
3.5 2.5 1.5
δ18O (‰)

Figure 7. Stable isotope results of Atlantic Site 1264. Blue lines always represent oxygen isotopes, orange line always represents carbon isotopes. Dark colours represent results from this study, light colours represent results from Liebrand et al., 2011. A. wavelet analysis of the carbon isotope record. Removal of > 0.5 Myr periodicities using a notch filter (Paillard et al., 1996) (*f*: 0.0, bw: 2.0) and normalization. Black line represents 95% confidence interval. B. Carbon isotope record. C. Gaussian filter (~41 kyr, *f*: 24.4, bw: 3.0) of oxygen isotope (blue) and carbon isotope (orange) record. D. Gaussian filter (~100 kyr, *f*: 10.0, bw: 2.0) of oxygen isotope (blue) and carbon isotope (orange) record. E. Oxygen isotope record. F. Same as A., for the oxygen isotope record. Black dotted line represents ~2.4 Myr eccentricity modulator, after Liebrand et al., 2011). G. and H., Phase wheel represents phase relation between the oxygen and carbon isotope record. 360 ° represents one full cycle. Phase lag increases clockwise. G. 400 kyr, H. 100 kyr.

4.3 Wavelet analysis

Wavelet provides an indication about the cycles playing a role in different parts the records (~24 – 17 Ma) (figure 7). The black line in both plots shows the 95 % confidence interval of the wavelet analysis. Liebrand et al. (2011) noted the dominance of the long-term eccentricity-related variability and the less profound influence (in distinct periods) of the short-term eccentricity related variability in both the $\delta^{13}C$ and $\delta^{18}O$ records. In this study, the dominance of the long-term eccentricity cycle is identified for both records (figure 7a and 7f). The influence of the short-term eccentricity is also identified. Filtering indicates that the interval ~17.8 to 17.0 Ma is dominated by the short-term eccentricity related variation in $\delta^{13}C$ values, while the variation in the $\delta^{13}C$ values during period ~19.0 Ma to 17.8 Ma is dominated by the long-term eccentricity cycle. The wavelet analysis confirms these observations. In both wavelet plots, the power of the long-term eccentricity cycle decreases between ~18 and 17 Ma, while in both plots, the power of the short-term eccentricity increases in the same interval. Sites 1090, 926 and 929 do not show these intervals dominated by the short-term eccentricity cycle. Probably Site 1264 is more vulnerable for dissolution due to its shallow position (1 – 1.5 km less deep) (Liebrand et al., 2011). Both wavelet plots also indicate some influence 40 kyr obliquity band.

In both records, eccentricity is modulated by the ~2.4 Myr eccentricity modulator. Since a ~2.4 eccentricity modulator minimum is identified at ~21 Ma, the next minimum is expected halfway between 19 and 18 Ma (figure 7).

4.4 Phase relations

For the period ~24.0 to 19.0 Ma, Liebrand et al. (2011) calculated the lag between both records for the long-term (400 kyr) and short-term (~125 kyr and ~95 kyr). In this study, for the long term eccentricity component between ~20 and 16.97 Ma, the lag between the two records is about ~–38.7 ° (figure 7g). This means that the long term eccentricity component of the $\delta^{13}C$ record lags the lags the long term eccentricity component of the $\delta^{18}O$ record ~43 kyr. which is very similar to the ~36 kyr lag of Liebrand et al. (2011). Since the two different short-term cycles are not recognizable as such in the $\delta^{18}O$ record, I choose to calculate the phase lag for the ~100 kyr eccentricity cycle, which is a combination of both the ~125 kyr and the ~95 kyr eccentricity cycle (figure 7h).. The phase lag between the $\delta^{18}O$ record and the $\delta^{13}C$ record for the 100 kyr eccentricity component is about ~-12.0 °, which means the short-term eccentricity component of the $\delta^{13}C$ record lags the short-term eccentricity component of the $\delta^{18}O$ record about 3 kyr for, which falls well between the 5 kyr and 0 kyr lags for the 95 kyr and 100 kyr short-term eccentricity cycle components calculated by Liebrand et al. (2011).

5 Discussion

5.1 Oxygen and carbon isotopic events

5.1.1 MMCO and Monterey event

Both the onset of the MMCO and the Monterey event have been identified as respectively negative and positive shifts in respectively the oxygen and carbon isotope records of Site 1264. The MMCO is characterized by low Antarctic ice volumes and relatively high bottom water

temperatures (Zachos et al., 2001b). Billups et al. (2004) identified a "negative" shift in oxygen isotope record of Site 1090, but they did not identify the MMCO, possibly because there is a "positive" shift at ~16.3 Ma. Zachos et al. (2001b) indicated this positive shift as well. Both shifts are part of the lead up to the MMCO. A lithostratigraphic study of ANDRILL core AND-2A revealed a similar trend, a significant amount of Antarctic ice retreat has been recorded between ~17.35 and 17.3 Ma. This has been associated with the Onset of the MMCO (Sandroni and Talarico, 2011; Fielding et al., 2011). Besides the MMCO, Billups et al. (2004) indicated the "positive" carbon isotope shift which is the onset of the Monterey event, although it is not called the Monterey event. This research indicates that both shifts recorded are because of global rather than local events. At Site 1264, the initiation of MMCO is slightly earlier than at Site 1090, ~17.34 Ma compared to ~17.26 Ma. The same is the case for the onset of the Monterey event, initiating at ~17.8 Ma at Site 1264 and ~17.6 Ma at Site 1090. Site 1090 is located deeper and more towards the south, and is influenced by different water masses. As a result, the "negative" shift in oxygen isotopes initiates at a slightly different moment. The results of this study are compared to the results of the Site 1090 and the results of Site 926. Since these sites are all located in the southern Atlantic ocean, the global implication of these results might be limited. The oxygen and carbon isotope records of Site 1264 match well to the $\delta^{18}O$ and $\delta^{13}C$ records of the Sites 1090 and 926, which indicates the global character of the events. Although the records match well, the $\delta^{18}O$ records of sites 1090 and 1264 are generally heavier than the $\delta^{18}O$ record of Site 926. Intra- and interbasinal differences in between oxygen isotopes records of different sites have been reported before, possibly due to the presence of different water masses (Pekar and DeConto, 2006, Cramer et al., 2011) The relative heaviness of the Site 1264 $\delta^{13}C$ record is explained by the relative shallow position of Site 1264, where it is bathed in a nutrient depleted intermediate water mass (Liebrand et al., 2011).

5.1.2 Mi-events

De Boer et al. (2010) created a set of 1-D ice sheet models to show that during the mid-Miocene, the oxygen isotope values were predominantly dependant on changes in ice volume than changes in bottom-water temperature. Lithostratigraphic analysis of ANDRILL drillcore AND-2A provided evidence for climatic fluctuations and related ice sheet expansions and contractions, accompanied by substantial sea-level changes during the early to middle-Miocene (~20.2 – 14.2 Ma). Seventy-four high-frequency (Milankovitch time scales) glacimarine cycles have been identified during this period (Fielding et al., 2011). This indicates the importance of ice volume on the mid-Miocene $\delta^{18}O$ record.

Liebrand et al. (2011) reports that major ice-sheet expansions coincide with 400 kyr eccentricity minima, during these times the ~100 kyr cycle is suppressed. They suggest that the major ice-sheet expansions are modulated by the long term obliquity component and eccentricity modulator (resp. 1.2 and 2.4 Myr), because major ice-sheet expansions do not occur at every minimum in the 400 kyr eccentricity cycle. The link between ice sheet expansion and the two modulators is, except for the Mi-1 event, yet to inconsistent to suggest a strong causal relationship between them. The Mi-1 event is also identified in the records from site 926. The astronomical solution La2004 (Laskar et at., 2004) shows a node in long term obliquity amplitude modulation during the Mi-1 event. In previous astronomical solutions, this node was more pronounced, similar to prior and later long-term obliquity amplitude nodes. As a result, further pre-conditioning is required to produce such an extreme event like the Mi-1 event (Pälike et al., 2006 after DeConto and Pollard, 2003). One possibility is a decrease of the atmospheric CO_2 level around the Mi-1 event. This indicates a non-linear response between astronomic cycles and climate.

Although no major Mi glaciation event occurred during the interval ~19 - 17 Ma (e.g. Mi-1, Mi-2; Miller et al., 1991), two smaller episodes of glaciation (Mi sub-events) are identified in the $\delta^{18}O$ record of Site 1090 for this time interval: the Mi-1ab and Mi-1b

events (Miller et al., 1991; Wright and Miller, 1993; Billups et al., 2002; Pekar and DeConto, 2006). Billups et al. (2002), dated the Mi-1b event at ~18.0 Ma, but more recently, this event has been dated at ~17.8 Ma, while the Mi-1ab event has been dated at ~18.4 Ma (Pekar and DeConto, 2006). A lithologically diverse facies including basal clasts and diamicties indicated ice proximal conditions which have been interpret as the Mi-1b event (Fielding et al., 2011). Both events have been identified in the oxygen isotope record of Site 1090. The δ18O record of Site 1264 at ~18.4 Ma is characterized by maximum of δ18O values, which correlates to the Mi-1ab event (figure 7e). The oxygen isotope record reaches a maximum value of ~ 2.80 ‰. At ~17.8 Ma, the oxygen isotope record is characterized by another maximum, which correlates to the Mi-1b event. A maximum oxygen isotope record of 2.65 ‰ is reached at ~17.8 Ma. During both the Mi-events recorded in this part of the record, the maximum $\delta^{18}O$ value is less than the maximum of 2.9 ‰ at Site 1090 (Pekar and DeConto, 2006). The latter site is located at a much deeper, southwards position and as a result is most likely affected by the cold and dense Antarctic water (e.g., the proto AABW), (Pekar and DeConto, 2006). These two Mi-events are characterized by maxima in the $\delta^{18}O$ record, which is rather low compared to the other Mi-events. At Site 1090, $\delta^{18}O$ values well above 3 ‰ are reached (Pekar and DeConto, 2006). The duration of the Mi-events identified in the oxygen isotope record of Site 1264 is well above the sampling resolution of this record (70 – 80 kyr). In the interval 18.9 – 16.97 Ma, the $\delta^{18}O$ record shows multiple positive excursions with maxima comparable to those of the Mi-1ab and Mi-1b events. This suggest glaciation events similar to the Mi-1ab and Mi-1b events occurred during this period. It also questions the validity of the identification of both Mi-events. One question is how the ~2.4 Myr eccentricity of the modulator influences these Mi-events? Liebrand et al. (2011) report a ~2.4 Myr eccentricity modulator minimum at ~21 Ma, which implies that the next minimum is at ~18.6 Ma. The M-1ab δ18O maximum at ~18.4 Ma could be influenced by this eccentricity modulator minimum. This is supported by the observation that the three subsequent $\delta^{18}O$ maxima after the eccentricity modulator minimum (~18.6, 18.4 and 18.2 Ma), become increasingly heavy. These minima are ~200 kyr apart, which suggest a weak long-term eccentricity cycle, but can explain the power spectral peak around 200 kyr (figure 6e). The reason for the 200 kyr separations remains unclear. The Mi-1ab event at ~18.4 Ma is part of the transition from a long-term eccentricity minimum to a maximum (figure 7e and 7f). In the original record, it is identified as a maximum within a minimum. This is an indication that the power of the long term eccentricity cycle is suppressed, which made it possible for the Mi-1ab event to occur (on a short-term eccentricity time scale).

5.2 Link between the $d^{18}O$ and $d^{13}C$ records

The main question remains, how does the link between the eccentricity cycle and cycles in carbon isotope ratios work? The coherence between the eccentricity cycle, δ18O and δ13C records (in this and other studies) indicates a strong coupling between changes in the carbon budget and the different climate states (Zachos et al., 2001; Pälike et al., 2006b; Liebrand et al., 2011). Insolation is mainly influenced by amplitude variation on the precession and obliquity frequency time scales. For both the early and middle Miocene (this research and Liebrand et al., 2011), power spectra and wavelet analysis indicate the dominance of both long and short term eccentricity frequencies for the oxygen and carbon isotope records. As a result, a non-linear system is required to transfer power from the precession and obliquity cycles to the eccentricity band (Liebrand et al., 2011). The dominant imprint of long and short term eccentricity and the weak imprint of obliquity on both records of Site 1264 is unexpected, considering the dominance of the obliquity for the records of Site 926. There could be a link to different water masses due to different positions of the two sites (Liebrand et al., 2011). During the early to mid-Miocene, the carbon isotope and oxygen isotope records of Site 1264 match well through time, although the onset of the MMCO and the Monterey event do not occur at the same time, ~17.3 Ma compared to ~17.8 Ma. This confirms a non-linear, but coupled response of the carbon and

oxygen isotopes to environmental changes. The "positive shift" in carbon the carbon isotope record suggests a change in global carbon budget. Holbourn et al. (2007) recognise three different climate phases during the mid-Miocene: I. prior to 14.7 Ma, a climatic optimum (the MMCO), characterized by low ice volume and prominent variability on long- and short-term timescales, II. from 14.7 to 13.9, obliquity modulated cooling, ending with a rapid increase in ice volume and global cooling, which initiates at the onset of the last and most pronounced $\delta^{13}C$ increase, III. after 13.9 Ma, an "Icehouse" mode, with the imprint of the short-term eccentricity. While the positive shift in the carbon isotope record suggest the drawdown atmospheric CO_2, the MMCO suggest the opposite. This implies that the full extent Monterey event did not occur before or during the MMCO, which is also suggested by Holbourn et al. (2007).

When taking the long residence time of carbon in the oceans (~ 10^5 yr) into account, the phase lag of the carbon isotope record compared to the oxygen isotope record (~43 kyr) is in accordance to the idea that orbital changes lead, and might even drive, changes in the ocean carbon budget (Zachos et al., 2001). Pälike et al. (2006b) used simple box model experiments to show that seasonal insolation cycles can drive changes in the biosphere productivity and carbon burial rate on long-term eccentricity timescales due to the long residence time of carbon in the ocean. The amount atmospheric CO_2 depends on the amount of carbon burial, as more carbon burial leads to increased drawdown of atmospheric CO_2 level. These box model experiments also showed that when the atmospheric CO_2 level is close to a specific threshold, the onset of major glaciation events is triggered by astronomical forcing rather than the exact timing of the reduction of atmospheric CO_2 levels. Carbon burial may also be increased because of enhanced upwelling intensity due to a stronger meridional temperature gradient during glacial phases (Liebrand et al., 2011). On the other hand, productivity may have increased during glacial times due to erosion of the continental shelves. This is supported by evidence from benthic foraminifer accumulation rates during the Oligocene/Miocene boundary. An in-phase relationship between changes in foraminifer accumulation rates and long- and short-term eccentricity was found (Liebrand et al. 2011; Dieter Haass et al., 2011). Since the record of Dieter-Haass et al. (2011) does not extend up to the Mi-1ab and Mi-1b events, it is unclear whether the same is the case for the extended part of the oxygen isotope record of Site 1264 (Dieter-Haass et al., 2011). The Oligocene/Miocene paleoproductivity record from Site 926 contains a significant variance on both the long- and short-term eccentricity timescales, which is coherent with the $\delta^{18}O$ and $\delta^{13}C$ records for the same site (Dieter-Haass et al., 2011). A fundamental interaction of solar forcing, glacial events and the carbon cycle is suggested by the response of the climate system to the complex orbital variations, with the main variations in the global carbon cycle driven by solar insolation biosphere contraction and expansion (Pälike et al., 2006b).

5.3 Future work

The next steps for this research should answer two main questions: how do the MMCO and Monterey event at Site 1264 continue into the mid-Miocene? What is the relationship between the carbon isotope record and oxygen isotope record during the Mid-Miocene?
Since this research only reveals the onset of the onset of both the MMCO and Monterey event, the first step should be to extend the oxygen and carbon isotope records to at least ~15.0 Ma to capture the MMCO, but preferably it should be extended to ~13.5 Ma, to record the full extent of the Monterey event. To test the analytical precision of the mass spectrometer, some samples should be measured again. The relationship between the carbon isotope and oxygen isotope records is still widely discussed within the literature, and extended oxygen and carbon isotope records from Site 1264 could contribute to this discussion. In order to gain more insight into the oxygen isotope variations, the $\delta^{18}O$ record could be separated into the temperature signal (δ_T) and the ice volume signal (δ_w). A Mg/Ca ratio study could be carried out. Mg/Ca ratios

can be used to extract the temperature signal out of an oxygen isotope record (Nürnberg, 1995). These studies could add to the question how the mid-Miocene oxygen isotope record and the MMCO are influenced by changes in the global carbon cycle. Power spectral analysis combined with wavelet analyses of ice volume signal could be used to reveal the behaviour of the Antarctic ice sheet.

6 Conclusions

The onset of the Mid Miocene Climatic Optimum has been identified at ~17.34 Ma in the extended part of oxygen isotope record Site 1264. The timing of onset of the MMCO identified in the oxygen isotope record of Site 1264, is in agreement to lithostratigraphic analysis of ANDRILL core AND-2A, where the onset of the MMCO is identified at 17.35 Ma. The timing of the onset of the MMCO at Site 1090 is slightly later, at ~17.26 Ma. In the extended part of the carbon isotope record, the onset of the Monterey event has been identified at ~17.8 Ma. The amplitude of the extended $\delta^{18}O$ and $\delta^{13}C$ records of Site 1264 are dominated by variations on the long-term eccentricity time-scales, although a prominent influence of the short-term eccentricity cycle has been observed too. The importance of these records comes out in both the power spectral analysis and the wavelet analyses. Both records behave in a similar way, which points to a coupled response of the records to environmental changes. The shift in the carbon isotope record suggest a change in the global carbon cycle. This, combined with the shift in the oxygen isotope records, suggest a non-linear response of both records. The carbon isotope records lags the oxygen isotope record by about 43 kyr, which is in agreement to the lag between the two records in other intervals of Site 1264.

Although the extended oxygen isotope record of Site 1264 is not part of any major mi-events, 2 sub Mi-events have been identified, at 18.4 and 17.8 Ma. These are Mi-1ab and Mi-1b respectively. This is in agreement to other sites. A long-term eccentricity modulator minimum is predicted at 18.6 Ma. The Mi-1ab glacial event could possibly be related to this minimum.

Acknowledgments

First of all, I would like to thank Lucas Lourens for providing me the opportunity to do this research. I would also like to thank him for his help when I did not know what to do. Besides Lucas Lourens, I would like to thank Helen Bedow, for always being there for me in case I needed help. I would also like to thank Arnold van Dijk and Dominica Krasnajuk for their help with the mass-spectrometer and the samples. Last but not least, I would like to thank my friends for the coffee breaks. Last but not least: Jan, thanks for teaching me how to work with Adobe Illustrator.

References

Billups, K., Channell, J. E. T., & Zachos, J. (2002). Late Oligocene to early Miocene geochronology and paleoceanography from the subantarctic South Atlantic. *Paleoceanography, 17*, 1–11.

Billups, K., Pälike, H., Channell, J. E. T., Zachos, J. C., & Shackleton, N. J. (2004). Astronomic calibration of the late Oligocene through early Miocene geomagnetic polarity time scale. *Earth and Planetary Science Letters*, *224*, 33–44. doi:10.1016/j.epsl.2004.05.004

Bowles, J. (2006) Data report: revised magnetostratigraphy and magnetic mineralogy of sediments from Walvis Ridge, Leg 208, in: Proc. ODP, Sci. Results, 208: College Station, TX (Ocean Drilling Program), edited by: Kroon, D., Zachos, J. C., and Richter, C., 1–24, doi:10.2973/odp.proc.sr.208.206.2006.

Cramer, B. S., Toggweiler, J. R., Wright, J. D., Katz, M. E., & Miller, K. G. (2009). Ocean overturning since the Late Cretaceous: Inferences from a new benthic foraminiferal isotope compilation. *Paleoceanography*, *24*, PA4216, doi:10.1029/2008PA001683.

Cowling, S.A. (1999). Plants and Temperature- CO_2 Uncoupling. *Science, 285*, 1500–1501.

De Boer, A. M., Sigman, D. M., Toggweiler, J. R., & Russell, J. L. (2007). Effect of global ocean temperature change on deep ocean ventilation. *Paleoceanography*, *22*, PA2210. doi:10.1029/2005PA001242

DeConto, R.M., Pollard, D. (2003). Rapid Cenozoic glaciation of Antarctica triggered by declining atmospheric CO_2. *Nature, 421*, 245–249.

Dieter-Haass, L., Billups, K., & Emeis, K. (2011). Enhanced paleoproductivity across the Oligocene/Miocene boundary as evidenced by benthic foraminiferal accumulation rates. *Palaeogeography, Palaeoclimatology, Palaeoecology*, *302*, 464–473. doi:10.1016/j.palaeo.2011.02.006

Fielding, C. R., Browne, G. H., Field, B., Florindo, F., Harwood, D. M., Krissek, L. a., Levy, R. H., et al. (2011). Sequence stratigraphy of the ANDRILL

AND-2A drillcore, Antarctica: A long-term, ice-proximal record of Early to Mid-Miocene climate, sea-level and glacial dynamism. *Palaeogeography, Palaeoclimatology, Palaeoecology*, *305*, 337–351. doi:10.1016/j.palaeo.2011.03.026

Flower, Benjamin P, & Kennett, J. P. (1993). Relations between Monterey Formation deposition and middle Miocene global cooling: Naples Beach section, California. *Geology, 21,* 877-880.doi:10.1130/0091-7613(1993)021<0877

Flower, B P, & Kennett, J. P. (1993b). Middle Miocene ocean-climate transition: high-resolution oxygen and carbon isotopic records from the Deep Sea Drilling Project Site 588A, Southwest Pacific, *8*, 811–843.

Flower, B.P., & Kennett, J. P. (1994). The middle Miocene climatic transition: East Antarctic ice sheet development, deep ocean circulation and global carbon cycling. *Paleobiology, Paleoclimatology, Paleoecology, 108,* 537-555.

Foster, G.L., Lear, C.H., & Rea, J.W.B. (2012). The evolution of pCO_2, ice volume and climate during the middle Miocene. *Earth and Planetary Science Letters, 341-344,* 243-254.

Henrot, A., & Franc, L. (2010). Effects of CO 2 , continental distribution, topography and vegetation changes on the climate at the Middle Miocene : a model study. *Climate of the Past Discussions, 6,* 489-535.

Holbourn, A., Kuhnt, W., Schulz, M., Flores, J.-A., & Andersen, N. (2007). Orbitally-paced climate evolution during the middle Miocene "Monterey" carbon-isotope excursion. *Earth and Planetary Science Letters*, *261*, 534–550. doi:10.1016/j.epsl.2007.07.026

IPCC, 2007. Climate Change 2007: The Scientific Basis. Contribution of Working Group 1 to the Fourth Assessment Report of the Intergovernmental Panel on Climate Change. *Cambridge Univ. Press, New York*.

Kürschner, W.M., Kvaček, Z., & Dilcher, D.L. (2008). The impact of Miocene atmospheric carbon dioxide fluctuations on climate and the evolution of terrestrial ecosystems, *Geology (PNAS), 105,* 449-453.

Kürschner, W. M., & Kvaček, Z. (2009). Oligocene-Miocene CO2 fluctuations, climatic and palaeofloristic trends inferred from fossil plant assemblages in central Europe. *Bulletin of Geosciences*, *84*,189–202. doi:10.3140/bull.geosci.1091.

Laskar, J., Robutel, P., Joutel, F., Gastineau, M., Correia, A. C. M., & Levrard, B. (2004). Long-term numerical solution for the insolation quantities of the Earth. *Astronomy & Astrophysics, 285,* 261–285. doi:10.1051/0004-6361.

Laskar, J., Fienga, A., Gastineau, M., & Manche, H. (2011). La2010: a new orbital solution for the long-term motion of the Earth. *Astronomy and Astrophysics, 532,* A89.

Lear, C. H. (2000). Cenozoic Deep-Sea Temperatures and Global Ice Volumes from Mg/Ca in Benthic Foraminiferal Calcite. *Science*, *287*, 269–272. doi:10.1126/science.287.5451.269.

Liebrand, D., Lourens, L. J., Hodell, D. A., De Boer, B., Van de Wal, R. S. W., & Pälike, H. (2011). Antarctic ice sheet and oceanographic response to eccentricity forcing during the early Miocene. *Climate of the Past*, *7*, 869–880. doi:10.5194/cp-7-869-2011

Miller, K. G., Wright, J. D., & Fairbanks, G. (1991). Unlocking the Ice House: Oligocene-Miocene Oxygen Isotopes, Eustasy, and Margin Erosion. *Journal of geophysical research*, *96*, 6829–6848.

Mosbrugger, V., Utescher, T., & Dilcher, D. L. (2005). Cenozoic continental climatic evolution of Central Europe. *PNAS*, *102*, 14964–14969. doi:10.1073/pnas.0505267102

Nürnberg, D. (1995). Magnesium in tests of *Neogloboquadrina pachyderma* sinistral from high northern and southern latitudes, *Journal of Foraminiferal research, 25*, 350-368.

Pagani, M., Arthur, M. A., & Freeman, K. H. (1999). Miocene evolution of atmospheric carbon dioxide. *Paleoceanography, 14*, 273–292.

Paillard, D., Labeyrie, L., & Yiou, P. (1996). Macintosh program performs time-series analysis. *Eos Trans*, *AGU, 77*, 379.

Pälike, H., Frazier, J., & Zachos, J. C. (2006a). Extended orbitally forced palaeoclimatic records from the equatorial Atlantic Ceara Rise. *Quaternary Science Reviews*, *25*, 3138–3149. doi:10.1016/j.quascirev.2006.02.011

Pälike, H., Norris, R. D., Herrle, J. O., Wilson, P. A, Coxall, H. K., Lear, C. H., Shackleton, N. J., Tripati, A.K., & Wade, B.S. (2006b). The heartbeat of the Oligocene climate system. *Science*, *314*, 1894–1898. doi:10.1126/science.1133822

Pearson, P. N., & Palmer, M. R. (2000). Atmospheric carbon dioxide concentrations over the past 60 million years. *Nature*, *406*, 695–9. doi:10.1038/35021000

Pekar, S. F., & DeConto, R. M. (2006). High-resolution ice-volume estimates for the early Miocene: Evidence for a dynamic ice sheet in Antarctica. *Palaeogeography, Palaeoclimatology, Palaeoecology*, *231*(1-2), 101–109. doi:10.1016/j.palaeo.2005.07.027

Royer, D. L., Wing, S. L., Beerling, D. J., Jolley, D. W., Koch, P. L., Hickey, L. J., & Berner, R. A. (2001). Paleobotanical evidence for near present-day levels of atmospheric Co2 during part of the tertiary. *Science , 292*, 2310–2313. doi:10.1126/science.292.5525.2310

Sandroni, S., & Talarico, F. M. (2011). The record of Miocene climatic events in AND-2A drill core (Antarctica): Insights from provenance analyses of basement clasts. *Global and Planetary Change*, *75*, 31–46. doi:10.1016/j.gloplacha.2010.10.002

Shackleton, N. J. (1974). Attainment of isotope equilibrium between ocean water and the benthonic foraminifera genus *uivergerina*: isotopic changes in the ocean during the last glacial. *Colloq. Int. Ctr. National Rech. Sci., 219,* 203–209.

Shackleton, N.J., Backman, J., Zimmerman, H., Kent D.V., Hall, M.A., Roberts, D.G., Schnitker, D., Baldauf, J.G., Desprairies, A., Homrighausen, R., Huddleston, P.,. Keene, J.B., Kaltenback, A.J., Krumsiek, K.A.O., Morton, A.C., Murray, J.W., & Westberg-Smith, J. (1984). Oxygen isotope calibration of the onset of ice-rafting and history of

glaciation in the North Atlantic region. *Nature, 307*, 620-623.

Sheldon, N. D. (2006). Using paleosols of the Picture Gorge Basalt to reconstruct the middle Miocene climatic optimum, *Paleobios, 26*, 27–36.

Toggweiler, J. R., and B. Samuels. (1998). On the ocean's large-scale circulation near the limit of no vertical mixing, *Journal of physical oceanography, 28,* 1832 – 1852, doi:10.1175/1520-0485(1998) 028<1832:OTOSLS>2.0.CO;2.

Tong, J. a., You, Y., Müller, R. D., & Seton, M. (2009). Climate model sensitivity to atmospheric CO2 concentrations for the middle Miocene. *Global and Planetary Change*, *67*), 129–140. doi:10.1016/j.gloplacha.2009.02.001

Vincent, E., & Berger, W.H., 1985. Carbon dioxide and polar cooling in the Miocene: the Monterey hypothesis. In: Sundquist, E.T., Broecker, W.S. (Eds.), The carbon cycle and atmospheric CO2: natural variations Archean to present, *AGU, Washington, DC*, 455–468.

Wright, J.D., Miller, K.G., & Fairbanks, R.G. (1992). Early and middle Miocene stable isotopes: implications for deepwater circulation and climate. *Paleoceonography, 7*, 357–389.

Wright, J.D., & Miller, K.G. (1993). Southern ocean influences on late Eocene to Miocene deepwater circulation. *Antarctic research series, 60*, 1-25.

You, Y., Huber, M., Müller, R. D., Poulsen, C. J., & Ribbe, J. (2009). Simulation of the Middle Miocene Climate Optimum. *Geophysical Research Letters*, *36*, L04702. doi:10.1029/2008GL036571.

You, Y. (2010). Climate-model evaluation of the contribution of sea-surface temperature and carbon dioxide to the Middle Miocene Climate Optimum as a possible analogue of future climate change. *Australian Journal of Earth Sciences*, *57*, 207–219. doi:10.1080/08120090903521671.

Zachos, J C, Shackleton, N. J., Revenaugh, J. S., Pälike, H., & Flower, B. P. (2001). Climate response to orbital forcing across the Oligocene-Miocene boundary. *Science, 292*, 274–278. doi:10.1126/science.1058288

Zachos, J., Pagani, M., Sloan, L., Thomas, E., & Billups, K. (2001b). Trends, Global Rhythms, Aberrations to in global climate to present, *Science, 292*, 686–693.

Zachos, J. C., Kroon, D., & Blum, P. (2004). Shipboard Scientific Party: Proc. ODP, *Init. Repts., 208*, Ocean Drilling Program, College Station, TX doi:10.2973/odp.proc.ir.208.2004.

Attachment 1

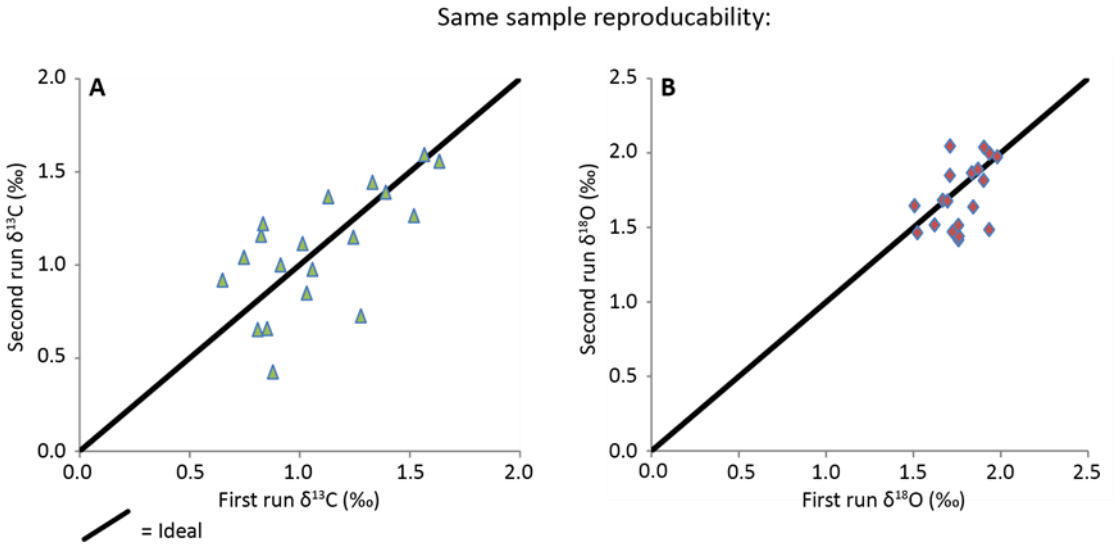

Same sample reproducability. The black line resembles the ideal situation. In each case, both samples ate measuder by the same mass-spectrometer. A. Same sample reproducability for carbon isotopes. B. same sample reoproducability for oxygen isotopes.

Attachment 2

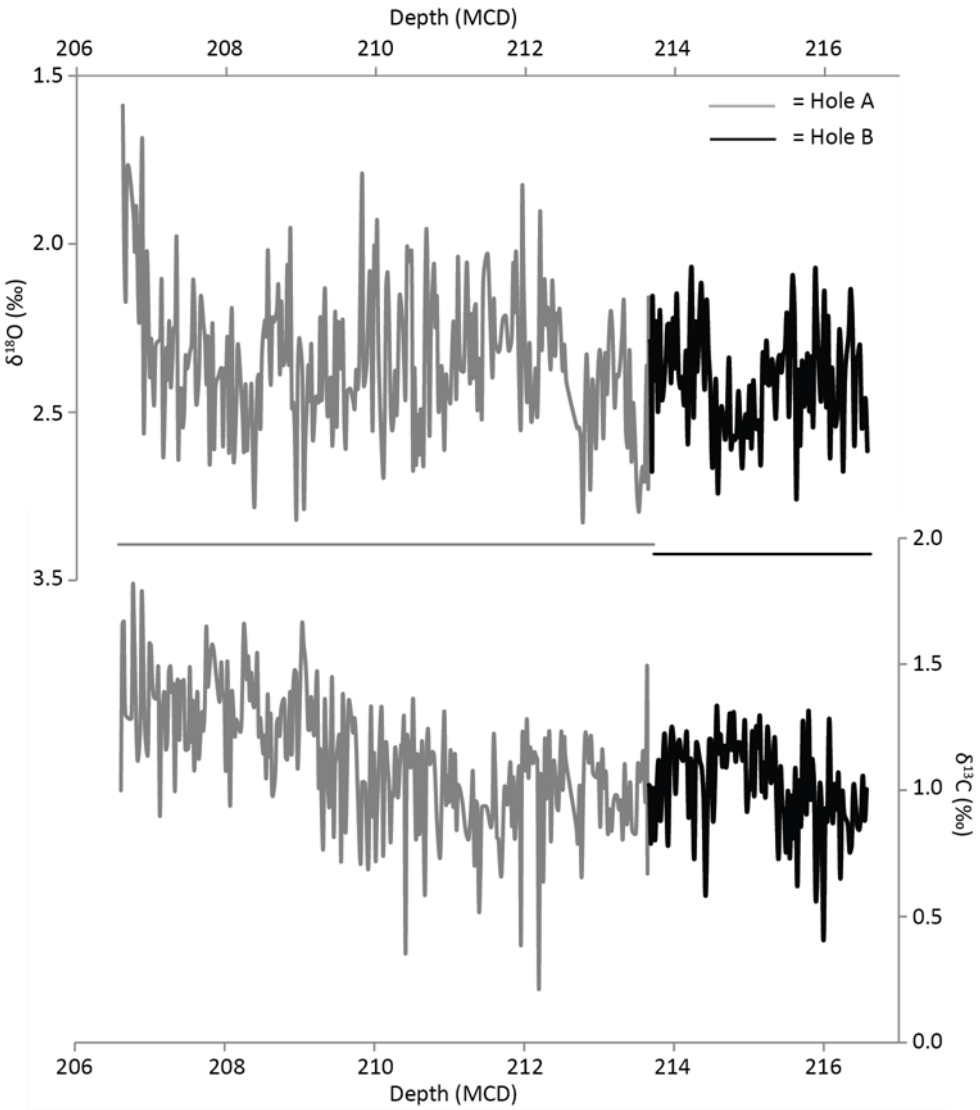

Oxygen and carbon isotopes, in depth. Light grey, samples from Hole A. Dark grey, samples from Hole B.